HHS Public Access

Author manuscript

J Alzheimers Dis. Author manuscript; available in PMC 2017 October 02.

Published in final edited form as:

J Alzheimers Dis. 2017 ; 57(2): 519–530. doi:10.3233/JAD-160981.

Amyloid Related Imaging Abnormalities (ARIA) in an Aged Squirrel Monkey with Cerebral Amyloid Angiopathy

Eric Heuer[1,2,*], **Jessica Jacobs**[2], **Rebecca Du**[1], **Silun Wang**[1], **Orion P. Kiefer Jr.**[1], **Amarallys F. Cintron**[1], **Jeromy Dooyema**[1], **Yuguang Meng**[1], **Xiaodong Zhang**[1], and **Lary C. Walker**[1,3]

[1]Yerkes National Primate Research Center, Emory University, Atlanta, GA 30329 USA

[2]Department of Psychology, University of Hawaii at Hilo, Hilo, HI 96783 USA

[3]Department of Neurology and Alzheimer's Disease Research Center, Emory University, Atlanta, GA 30322

Abstract

Amyloid-related imaging abnormalities (ARIA) in magnetic resonance imaging scans have emerged as indicators of potentially serious side effects in clinical trials of therapeutics for Alzheimer's disease. These anomalies include an edematous type (ARIA-E) that appears as hyperintense (bright) regions by T2-weighted MRI, and a type characterized by the deposition of hemosiderin (ARIA-H) that elicits a hypointense signal, especially in T2* and susceptibility-weighted imaging. ARIA in general has been linked to the presence of Aβ-type cerebral amyloid angiopathy, an accumulation of misfolded Aβ protein in the vascular wall that impairs the integrity of brain blood vessels. However, the pathobiology of ARIA remains poorly understood, in part due to the absence of an animal model of the disorder that would enable a contemporaneous analysis of tissue integrity in the affected region. Here we describe both ARIA-E and ARIA-H in an aged squirrel monkey (*Saimiri sciureus*), a nonhuman primate model of naturally occurring cerebral amyloid angiopathy. Histopathologic examination of the anomalous region revealed reactive astrocytosis and microgliosis, infiltration of systemic inflammatory/immune cells, damage to axons and myelin, and hemosiderin deposition. The disruption of axons in particular suggests that ARIA-E could have functional consequences for affected regions. The squirrel monkey model can be useful for studying the pathogenesis and long-term effects of ARIA, and for testing the safety and efficacy of emerging therapies for Alzheimer's disease.

Keywords

Alzheimer's disease; Amyloid-beta; ARIA-E; ARIA-H; inflammation; immunotherapy; MRI; vascular disease

[*]Corresponding author: Eric Heuer, Psychology Department, University of Hawaii at Hilo, 200 W. Kawaili St., Hilo, HI 96720, Phone: 808-932-7077, eheuer@hawaii.edu.

The authors declare no conflicts of interest.

The authors declare no competing financial interests.

1. Introduction

The accumulation of abnormally folded amyloid-β protein (Aβ) in the brain is an early and essential event in the pathogenesis of Alzheimer's disease (AD) [1–3]. A current experimental strategy to treat or prevent AD is active or passive immunization against Aβ [4–6]. The development of effective immunotherapies for AD, however, has been hindered by the appearance of anomalous magnetic resonance imaging (MRI) findings known as amyloid-related imaging abnormalities (ARIA) in some patients [7–12]. ARIA can consist of edema (ARIA-E) or microhemorrhage-related hemosiderin deposition (ARIA-H) in the brain. Spontaneous ARIA-E has been detected infrequently in AD patients, but its incidence increases significantly in patients undergoing anti-Aβ immunotherapy and possibly also secretase inhibition in treatment trials for AD [13]. In many instances, ARIA-E is thought to reflect transient edema that is not associated with long-term changes such as a breakdown of tissue integrity, but little direct information exists to confirm or refute this assertion [13].

Mounting evidence indicates that both ARIA-E and ARIA-H are associated with the presence of Aβ-type cerebral amyloid angiopathy (CAA) [13, 14], in which the accumulation of misfolded Aβ in and around blood vessels impairs the vascular wall [14, 15]. CAA is present to some degree in nearly all AD patients [16–18], and is severe in approximately 20% [19–21]. Anti-Aβ immunotherapy has been shown to reduce Aβ plaque load in AD patients [12, 22–24] and, later in the response to treatment, possibly CAA as well [14, 25]. In the first months following immunotherapy, postmortem histopathology suggests a redistribution of Aβ from the brain parenchyma to the vasculature [25], potentially increasing the risk of hemorrhagic stroke. Studies in Aβ-precursor protein-transgenic mouse models have supported the assertion that anti-Aβ immunization can induce microvascular hemorrhage that is linked to CAA [8], but ARIA *per se* has not been reported in rodent models.

Despite the problems that have beset immunotherapy trials, there have been hints that Aβ-immunotherapy might be clinically beneficial in some AD patients [12, 22], especially when administered early in the course of cognitive decline [26, 27]. ARIA is a potentially serious complication, however, and threatens to impede the development of disease-modifying therapies for AD [9, 20, 26]. The pathophysiology of ARIA remains poorly understood, in large part owing to the absence of a suitable animal model of the disorder [13]. In addition, because ARIA-E can be transitory in humans, there is little information on the histopathological basis of the imaging anomalies at the time the MRI is performed [13]. In the present study, we describe histopathological evidence for gliosis, inflammation, and white matter disruption by spontaneous ARIA-E and ARIA-H in an aged squirrel monkey, a nonhuman primate model of naturally occurring CAA [28–30].

2. Materials and Methods

2.1 Subjects

Four female squirrel monkeys (*Saimiri sciureus*) with known birthdates were analyzed (Table). Squirrel monkeys have a maximum lifespan of approximately 30 years [30, 31]; they express human-sequence Aβ [32] and begin to deposit the protein in the brain at around

13 years of age [28]. Two 19-year-old squirrel monkeys were from the University of Texas MD Anderson Research Center in Bastrop, Texas, and two animals aged 13 and 16 years were from the Yerkes National Primate Research Center of Emory University in Atlanta, Georgia. All experiments were conducted at the Yerkes Center in accordance with the NIH Guidelines for the Ethical Care and Use of Animal Subjects, and were approved by the Emory University Institutional Animal Care and Use Committee (IACUC).

2.2 MRI Data Acquisition

The subjects were initially sedated with ketamine (15 mg/kg, i.m.), placed on a temperature-controlled heating pad, and anesthetized with ~1% isoflurane delivered via a non-rebreathing circuit. The head was immobilized with a custom head holder, and the animals were placed in the prone position during MRI scanning. All major physiological parameters were monitored continuously (heart rate, respiratory rate, blood pressure, body temperature, end-tidal CO2 [EtCO2], peripheral oxygen saturation [SpO2]) and maintained within normal ranges throughout the scan.

MRI images were acquired using a 3T clinical scanner (MAGNETOM Trio, a TIM system, Siemens Healthcare, Erlangen, Germany) with a single-loop receive-only surface coil (ID=7 cm). T1-weighted images were collected using a 3D magnetization-prepared gradient-echo (MP-RAGE) sequence with the parameters: TR = 3000ms, TE = 3.81ms, FOV = 80mm × 80mm, flip angle = 8 degree, TI = 950ms, image matrix = 192 × 192, slice thickness = 0.42mm, 128 slices, bandwidth = 170 Hz, 3 averages.

T2-weighted images were acquired with a fast spin-echo sequence with TR = 8040ms, TE = 73 ms, FOV = 80mm × 80mm, data matrix = 256 × 256, turbo-factor = 17, 50 slices, slice thickness = 1mm, 4 averages.

T2*-weighted images (susceptibility-weighted images [SWI]) were collected using a 3D FLASH sequence with TR = 35ms, TE = 25 ms, FOV = 80mm × 80mm, data matrix = 256 × 256, flip angle = 15 degree, bandwidth = 150 Hz, 160 slices, slice thickness = 0.31 mm, 2 averages.

Diffusion tensor imaging (DTI) data were acquired using a single-shot EPI sequence with the following imaging parameters: TE = 104 ms, TR = 5000 ms, data matrix = 60 × 74, voxel size = 1.1 mm × 1.1 mm, 30 slices with thickness 1.1 mm, a b-value of 1000 s/mm^2 and 30 diffusion-encoding directions. DTI data sets were acquired with identical imaging parameters except for reversed phase-encoding direction for correcting susceptibility-related image distortions.

2.3 MRI Analysis

MR images were visually evaluated on the MRI scanner console and further analyzed using ImageJ (http://rsb.info.nih.gov/ij/index.html). Examination of images began with the identification and quantification of MR signal irregularities, which were described based on morphology and anatomical location. Analyses were performed by at least two individual raters to ensure an accurate assessment of the entire brain of each subject. The initial examination focused on major structural alterations that would indicate a significant pre-

existing condition (such as tumors or major infarcts), of which none were found. Subsequently, all images were inspected for the presence of abnormal MRI signals, which were defined *a priori* as being at least one mm in diameter (in-plane resolution) and being present in a minimum of three adjacent slices of the whole brain MRI. Once an anomaly was identified, its anatomical location, extent and nature were recorded for comparison to other MR modalities and to the histological brain sections.

DTI data were processed with FSL toolbox (FMRIB, Oxford). Susceptibility-related distortions in DTI data were corrected with TOPUP script in FSL. Diffusion-weighted imaging (DWI) representations were calculated by averaging the images of all 30 diffusion directions. Fractional anisotropy (FA), mean diffusivity (MD), and vector maps (showing the principal diffusion tensor direction) were calculated and displayed with FSL scripts.

2.4 Tissue Preparation and Histology

Immediately following *in vivo* imaging, the subjects were sedated with ketamine (15 mg/kg, i.m.), given an overdose of sodium pentobarbital (100 mg/kg i.v.), and, under deep anesthesia, transcardially perfused with cool (4–8°C), filtered phosphate-buffered saline (PBS) (pH 7.4) followed by 10% neutral buffered formalin (NBF). The brain was removed and post-fixed in 10% NBF for a minimum of one week. All brains were grossly normal and devoid of obvious external indications of disease or injury.

Brains were blocked into four coronal slabs, matching as closely as possible the slice plane in the MRI, and then cryoprotected for one week in 30% sucrose dissolved in PBS. The slabs were frozen on dry ice, and coronal sections were cut on a Microm HM 430 freezing-sliding microtome at 40μm thickness. Systematically selected sections were stained with hematoxylin & eosin (H&E), Perls' stain for ferric iron, thioflavin-S for amyloid, Luxol Fast Blue for myelin, or immunohistochemically for the following antigens: Aβ1-16 (antibody 6E10, Covance, Princeton, NJ), glial fibrillary acidic protein (GFAP) for astrocytes (Boehringer Mannheim, Indianapolis, IN), ionized calcium-binding adapter molecule 1 (IBA-1) for microglia (Wako Chemicals USA, Richmond, VA), CD68 for macrophages (Dako, Carpinteria, CA), CD3 for T lymphocytes (Abcam, Cambridge, MA), SMI-31 for phosphorylated neurofilaments (Covance), or CP13 for phospho-tau 202 (courtesy of Dr. Peter Davies, Feinstein Institute for Medical Research, Manhasset, NY, USA). Primary antibodies were detected using the avidin-biotin peroxidase method (Vectastain Elite ABC kits, Vector Laboratories, Burlingame, CA).

Immunostaining consisted of incubating tissue in 1% H_2O_2 for 30 minutes, then in 0.3% Triton X-100 for 10 minutes and 5% blocking serum for 30 minutes, all in Tris-buffered saline (TBS). Immunodetection of Aβ was enhanced by pre-treatment of the sections with formic acid (no other antigen required this step). Tissue was incubated with primary antibodies in TBS at 4°C, overnight. The following day, the tissue was washed in TBS and the antigens visualized with the ABC method using 3,3′-diaminobenzidine (DAB) as the chromogen. Some sections were counterstained with hematoxylin. Light-microscopic images were captured with an Aperio scanner (Leica Biosystems, Buffalo Grove, IL), a Leica DMLB microscope (Leica, Wetzlar, Germany) equipped with a Spot Flex digital camera (Diagnostic Instruments, Sterling Heights, MI), or with a Nikon Labophot

microscope (Tokyo, Japan) equipped with a Moticam 2500 camera (Vancouver, British Columbia, Canada). Aβ-immunoreactive parenchymal (plaque) and vascular (CAA) deposits were quantitatively assessed on a scale of 0 (none) to 4 (heavy) by consensus of three independent observers using photos of the different stages as standards.

3. Results

3.1 MRI of ARIA-E and ARIA-H

In the parieto-occipital lobes of 19-year-old squirrel monkey 2266, *in vivo* MR imaging revealed large, bilaterally asymmetric signal abnormalities that were consistent with ARIA-E and ARIA-H (Figures 1, 2). The ARIA-E-like T2-weighted signal hyperintensity encompassed the dorsomedial parieto-occipital white matter and (to a lesser extent) the gray matter of both hemispheres for approximately 8 mm in the rostrocaudal axis. T1-weighted structural images corresponding to the T2 hyperintense region demonstrated reduced white matter definition throughout the affected zone (Figure 2). Diffusion-weighted imaging showed evidence of increased mean diffusivity (Figure 1B) in the anomalous area. Affected sites had a corresponding reduction in fractional anisotropy (Figure 1C) and white matter directionality (Figure 1D) compared to the same regions in an unaffected animal of similar age (2276). Susceptibility-weighted imaging disclosed signal hypointensities consistent with ARIA-H that partially overlapped with the ARIA-E signal in the dorsal parieto-occipital lobes (Figure 2). Multiple MR modalities disclosed no similar signal abnormalities elsewhere in the brain, nor were any found in the other three animals analyzed.

3.2 Histopathologic Features of ARIA-E and ARIA-H

Aβ immunohistochemistry and thioflavin-S staining detected species-typical CAA throughout much of the forebrain in the affected animal (2266). In the region of the parieto-occipital lobes exhibiting signal anomalies by MRI, numerous amyloidotic large vessels were evident in the sulci, as were amyloidotic large and small vessels within the brain parenchyma (Figures 3,7). Compared to unaffected regions (Figure 4E,4G), the T2-weighted hyperintense ARIA-E region was marked by pronounced astrocytic and microglial hypertrophy (Figure 4D,4F) in the white matter and (to a lesser degree) the gray matter. Immunostaining for phosphorylated neurofilaments and Luxol Fast Blue staining of myelin showed evidence of axonal abnormalities and disruption of white matter integrity in the involved area (Figure 5).

The parieto-occipital sulcus (the caudomedial extension of the lateral cerebral fissure) was somewhat expanded and partly occupied by an abnormal cell-rich matrix that surrounded sulcal and penetrating blood vessels (Figure 6). Many of the vessels were immunoreactive for Aβ (Figure 7), and the penetrating branches exhibited characteristic cuffing by cells that were continuous with those in the sulcal material (Figure 6C), indicative of focal angiitis [33]. The cellular matrix contained profuse CD68-immunoreactive macrophages (Figure 6F) and CD3-positive lymphocytes (Figure 6G). The sulcal substance was accompanied by ferric iron-reactive hemosiderin (Figure 6D) that surrounded CAA-positive blood vessels (Figure 6E) and co-localized with the rostro-caudal extent of the hypointense MR signals detected by SWI.

In the oldest of the three other squirrel monkeys (animal 2276), the degree of CAA was similar to that in the ARIA-affected animal, whereas in the younger monkeys (2504 and 3237), CAA was less profuse (Table). None of the other animals showed ARIA-type imaging abnormalities or significant histopathological lesions, except for the presence of Aβ deposits. Periventricular white matter hyperintensities, as have been reported in humans with CAA [34], were not evident in any of the four subjects. None of the animals displayed evidence of sensorimotor deficits, but systematic behavioral testing that might have revealed subtle cognitive or sensory deficits was not undertaken.

4. Discussion

Amyloid-related imaging abnormalities are a significant impediment to the development of effective therapies for Alzheimer's disease [13]. To date, despite the availability of numerous genetically modified mouse models of AD-like pathology, no suitable model of ARIA has been identified. Here we describe an aged squirrel monkey with naturally occurring ARIA-E and ARIA-H that are linked histopathologically to CAA, gliosis, inflammation, iron deposition, and axonal abnormalities. The disruption of axons in particular indicates that ARIA-E may have significant, and possibly long-term, functional consequences for brain areas interconnected by the affected axons.

Earlier investigations showed that aging squirrel monkeys are particularly vulnerable to CAA [28–30], usually beginning around the age of 13 years [28]. In our experience, some degree of CAA is always present in squirrel monkeys after 15 years of age, and by the late teens it is severe and widespread, especially in the neocortex [29]. It is possible that ARIA is infrequent in normal aged squirrel monkeys, even when CAA is present; furthermore, some ARIA-E events might escape detection due to their apparently transient nature [13]. However, given the connection between ARIA and CAA in humans [13, 14], and the heightened incidence of ARIA in therapeutic trials of Aβ-immunotherapy [10, 12, 26, 35], the squirrel monkey could be a sensitive *in vivo* model for testing the safety of such therapies and for assessing possible long-term consequences arising from transient ARIA-E [13].

Along with CAA, the ARIA-affected brain region was marked by pronounced inflammation that included reactive gliosis in the parenchyma as well as infiltration of macrophages and lymphocytes into both the parenchyma and adjacent sulcus. In humans, idiopathic CAA-related inflammation is a rare disorder [36, 37] that manifests in various ways [38] and has been given a number of monikers, such as Aβ-related angiitis (ABRA), cerebral amyloid inflammatory vasculopathy, and others [39]. CAA-related inflammation in humans involves the incursion of inflammatory cells [36], and in many (but not all) cases, CAA-related inflammation responds favorably to immunosuppressive agents [36, 39, 40]. The extent to which the cellular inflammatory reaction *per se* contributes to the aberrant MRI signal hyperintensities in T2-weighted scans (as opposed to the contribution of vasogenic edema alone) is unknown. We also cannot know with certainty if the edematous imaging abnormality in the aged squirrel monkey represents a chronic process that is unrelated to the vascular amyloid. Experimental induction of ARIA-E in the squirrel monkey model, e.g., by administration of certain anti-Aβ antibodies, might help to gauge the contribution of

inflammatory cells both to the MR signal abnormality and to the disruption of tissue integrity. Furthermore, the timecourse of changes can be systematically monitored in the model, including behavioral proficiency and potential biomarkers in the CSF and blood. The model may also aid in determining why some ARIA patients suffer from significant cognitive impairment following treatment with anti-inflammatory/immunosuppressive agents [38, 41–44].

In humans, increased CAA and spontaneous ARIA have been associated with the apolipoprotein E-ε4 (*APOE4*) allele [14, 45]. In addition, All nonhuman primates studied thus far are homozygous for *APOE4* according to the standard (human) nomenclature, although a threonine rather than arginine at amino acid position 61 is thought to cause nonhuman primate ApoE4 to function similarly to ApoE3 [46], the most common human isoform. Further work is needed to determine whether the nonhuman primate type of ApoE4, which presumably is the ancestral form of the protein [47, 48], is a risk factor for CAA and ARIA.

Age-related cerebral Aβ deposition has been reported in several nonhuman primate species [49, 50] and in other mammals such as senescent dogs [51, 52]. Because CAA is common in many of these species [29, 30, 51, 53], it might be fruitful to determine whether they also are susceptible to ARIA in old age or as a result of experimental therapies.

Advances in high-field MRI techniques have continually lowered the threshold for detection of cerebrovascular abnormalities and their sequelae, but few studies have been able to determine the concurrent neuropathological correlates of ARIA-related changes, especially in the case of ARIA-E. The interpretation of MRI irregularities in humans is confounded by the often long interval between detection of ARIA in the living patient and subsequent histological assessment of tissue integrity in the region at autopsy. Additional obstacles to correlative analysis are long and variable postmortem intervals, the lack of consistency in tissue processing and fixation, and selection bias in the performance of autopsies. The limited information linking MRI signal anomalies to neuropathology has tended to rely largely on *ex vivo* imaging of postmortem brains, which may yield results that differ from those achieved *in vivo*, particularly with regard to edematous regions such as ARIA-E. For example, while T1-weighted scans are the standard for *in vivo* structural imaging, these same modalities do not yield reliably interpretable images when used on fixed tissue [54]. Sequential MR analysis of squirrel monkey brains *in vivo* and *ex vivo* can be used to determine the validity of *ex vivo* imaging of tissues from human subjects. An additional advantage of the squirrel monkey model is that the pathologic basis of MR imaging anomalies detected *in vivo* can be ascertained in near-real time.

Conclusions

We document the first known instance of naturally occurring ARIA in a nonhuman species. Both ARIA-E and ARIA-H were identified *in vivo* by 3T MRI in overlapping territories of the parieto-occipital lobes of an aged squirrel monkey with CAA. Histologically, the affected territories were marked by vascular Aβ deposition, focal hemosiderosis, reactive gliosis, disruption of axons and myelin, and the infiltration of inflammatory cells. As a

model of CAA and ARIA, the aged squirrel monkey could help to establish the probable nature and long-term consequences of ARIA in AD patients undergoing therapies designed to reduce the cerebral burden of aggregated Aβ [12], and to develop strategies for mitigating the impact of ARIA on the brain.

Acknowledgments

Grant Funding: This work was supported by the National Institutes of Health [R21NS077049, RR00165 and OD11132], as well as the MetLife Foundation and the Humboldt Foundation.

We gratefully acknowledge Lawrence E. Williams (UT MD Anderson Cancer Center) for providing aged animals, and Sudeep Patel, Ruth Connelly, and Doty Kempf (Yerkes Imaging Center) for expert assistance with MRI scans and animal care.

References

1. Holtzman DM, Morris JC, Goate AM. Alzheimer's disease: the challenge of the second century. Sci Transl Med. 2011; 3:77sr71.
2. Scheltens P, Blennow K, Breteler MM, de Strooper B, Frisoni GB, Salloway S, Van der Flier WM. Alzheimer's disease. Lancet. 2016
3. Selkoe DJ, Hardy J. The amyloid hypothesis of Alzheimer's disease at 25 years. EMBO Mol Med. 2016; 8:595–608. [PubMed: 27025652]
4. Lannfelt L, Relkin NR, Siemers ER. Amyloid-ss-directed immunotherapy for Alzheimer's disease. J Intern Med. 2014; 275:284–295. [PubMed: 24605809]
5. Wisniewski T, Goni F. Immunotherapy for Alzheimer's disease. Biochem Pharmacol. 2014; 88:499–507. [PubMed: 24412277]
6. Agadjanyan MG, Petrovsky N, Ghochikyan A. A fresh perspective from immunologists and vaccine researchers: active vaccination strategies to prevent and reverse Alzheimer's disease. Alzheimers Dement. 2015; 11:1246–1259. [PubMed: 26192465]
7. Black RS, Sperling RA, Safirstein B, Motter RN, Pallay A, Nichols A, Grundman M. A single ascending dose study of bapineuzumab in patients with Alzheimer disease. Alzheimer Dis Assoc Disord. 2010; 24:198–203. [PubMed: 20505438]
8. Pfeifer M, Boncristiano S, Bondolfi L, Stalder A, Deller T, Staufenbiel M, Mathews PM, Jucker M. Cerebral hemorrhage after passive anti-Abeta immunotherapy. Science. 2002; 298:1379. [PubMed: 12434053]
9. Arrighi HM, Barakos J, Barkhof F, Tampieri D, Jack C Jr, Melancon D, Morris K, Ketter N, Liu E, Brashear HR. Amyloid-related imaging abnormalities-haemosiderin (ARIA-H) in patients with Alzheimer's disease treated with bapineuzumab: a historical, prospective secondary analysis. J Neurol Neurosurg Psychiatry. 2016; 87:106–112. [PubMed: 25669746]
10. Wisniewski T, Drummond E. Developing therapeutic vaccines against Alzheimer's disease. Expert Rev Vaccines. 2016; 15:401–415. [PubMed: 26577574]
11. Piazza F, Winblad B. Amyloid-Related Imaging Abnormalities (ARIA) in Immunotherapy Trials for Alzheimer's Disease: Need for Prognostic Biomarkers? J Alzheimers Dis. 2016; 52:417–420. [PubMed: 27031492]
12. Sevigny J, Chiao P, Bussiere T, Weinreb PH, Williams L, Maier M, Dunstan R, Salloway S, Chen T, Ling Y, O'Gorman J, Qian F, Arastu M, Li M, Chollate S, Brennan MS, Quintero-Monzon O, Scannevin RH, Arnold HM, Engber T, Rhodes K, Ferrero J, Hang Y, Mikulskis A, Grimm J, Hock C, Nitsch RM, Sandrock A. The antibody aducanumab reduces Abeta plaques in Alzheimer's disease. Nature. 2016; 537:50–56. [PubMed: 27582220]
13. Sperling RA, Jack CR Jr, Black SE, Frosch MP, Greenberg SM, Hyman BT, Scheltens P, Carrillo MC, Thies W, Bednar MM, Black RS, Brashear HR, Grundman M, Siemers ER, Feldman HH, Schindler RJ. Amyloid-related imaging abnormalities in amyloid-modifying therapeutic trials: recommendations from the Alzheimer's Association Research Roundtable Workgroup. Alzheimers Dement. 2011; 7:367–385. [PubMed: 21784348]

14. Yamada M. Cerebral amyloid angiopathy: emerging concepts. J Stroke. 2015; 17:17–30. [PubMed: 25692104]
15. Biffi A, Greenberg SM. Cerebral amyloid angiopathy: a systematic review. J Clin Neurol. 2011; 7:1–9. [PubMed: 21519520]
16. Attems J, Jellinger KA. The overlap between vascular disease and Alzheimer's disease--lessons from pathology. BMC Med. 2014; 12:206. [PubMed: 25385447]
17. Vinters HV. Emerging concepts in Alzheimer's disease. Annu Rev Pathol. 2015; 10:291–319. [PubMed: 25387055]
18. Kapasi A, Schneider JA. Vascular contributions to cognitive impairment, clinical Alzheimer's disease, and dementia in older persons. Biochim Biophys Acta. 2016; 1862:878–886. [PubMed: 26769363]
19. Preston SD, Steart PV, Wilkinson A, Nicoll JA, Weller RO. Capillary and arterial cerebral amyloid angiopathy in Alzheimer's disease: defining the perivascular route for the elimination of amyloid beta from the human brain. Neuropathol Appl Neurobiol. 2003; 29:106–117. [PubMed: 12662319]
20. Weller RO, Boche D, Nicoll JA. Microvasculature changes and cerebral amyloid angiopathy in Alzheimer's disease and their potential impact on therapy. Acta Neuropathol. 2009; 118:87–102. [PubMed: 19234858]
21. Charidimou A, Gang Q, Werring DJ. Sporadic cerebral amyloid angiopathy revisited: recent insights into pathophysiology and clinical spectrum. J Neurol Neurosurg Psychiatry. 2012; 83:124–137. [PubMed: 22056963]
22. Gilman S, Koller M, Black RS, Jenkins L, Griffith SG, Fox NC, Eisner L, Kirby L, Rovira MB, Forette F, Orgogozo JM, Team ANS. Clinical effects of Abeta immunization (AN1792) in patients with AD in an interrupted trial. Neurology. 2005; 64:1553–1562. [PubMed: 15883316]
23. Ostrowitzki S, Deptula D, Thurfjell L, Barkhof F, Bohrmann B, Brooks DJ, Klunk WE, Ashford E, Yoo K, Xu ZX, Loetscher H, Santarelli L. Mechanism of amyloid removal in patients with Alzheimer disease treated with gantenerumab. Arch Neurol. 2012; 69:198–207. [PubMed: 21987394]
24. Lemere CA, Masliah E. Can Alzheimer disease be prevented by amyloid-beta immunotherapy? Nat Rev Neurol. 2010; 6:108–119. [PubMed: 20140000]
25. Boche D, Zotova E, Weller RO, Love S, Neal JW, Pickering RM, Wilkinson D, Holmes C, Nicoll JA. Consequence of Abeta immunization on the vasculature of human Alzheimer's disease brain. Brain. 2008; 131:3299–3310. [PubMed: 18953056]
26. Lemere CA. Immunotherapy for Alzheimer's disease: hoops and hurdles. Mol Neurodegener. 2013; 8:36. [PubMed: 24148220]
27. Delrieu J, Ousset PJ, Voisin T, Vellas B. Amyloid beta peptide immunotherapy in Alzheimer disease. Rev Neurol (Paris). 2014; 170:739–748. [PubMed: 25459121]
28. Walker LC, Masters C, Beyreuther K, Price DL. Amyloid in the brains of aged squirrel monkeys. Acta Neuropathol. 1990; 80:381–387. [PubMed: 2239150]
29. Elfenbein HA, Rosen RF, Stephens SL, Switzer RC, Smith Y, Pare J, Mehta PD, Warzok R, Walker LC. Cerebral beta-amyloid angiopathy in aged squirrel monkeys. Histol Histopathol. 2007; 22:155–167. [PubMed: 17149688]
30. Heuer E, Rosen RF, Cintron A, Walker LC. Nonhuman primate models of Alzheimer-like cerebral proteopathy. Curr Pharm Des. 2012; 18:1159–1169. [PubMed: 22288403]
31. Finch CE, Sapolsky RM. The evolution of Alzheimer disease, the reproductive schedule, and apoE isoforms. Neurobiol Aging. 1999; 20:407–428. [PubMed: 10604433]
32. Levy E, Amorim A, Frangione B, Walker LC. beta-Amyloid precursor protein gene in squirrel monkeys with cerebral amyloid angiopathy. Neurobiol Aging. 1995; 16:805–808. [PubMed: 8532114]
33. Oide T, Tokuda T, Takei Y, Takahashi H, Ito K, Ikeda S. Serial CT and MRI findings in a patient with isolated angiitis of the central nervous system associated with cerebral amyloid angiopathy. Amyloid. 2002; 9:256–262. [PubMed: 12557755]
34. Reijmer YD, van Veluw SJ, Greenberg SM. Ischemic brain injury in cerebral amyloid angiopathy. J Cereb Blood Flow Metab. 2015

35. Werring DJ, Sperling R. Inflammatory cerebral amyloid angiopathy and amyloid-modifying therapies: variations on the same ARIA? Ann Neurol. 2013; 73:439–441. [PubMed: 23526685]
36. Scolding NJ, Joseph F, Kirby PA, Mazanti I, Gray F, Mikol J, Ellison D, Hilton DA, Williams TL, MacKenzie JM, Xuereb JH, Love S. Abeta-related angiitis: primary angiitis of the central nervous system associated with cerebral amyloid angiopathy. Brain. 2005; 128:500–515. [PubMed: 15659428]
37. Nouh A, Borys E, Gierut AK, Biller J. Amyloid-Beta related angiitis of the central nervous system: case report and topic review. Front Neurol. 2014; 5:13. [PubMed: 24550886]
38. Moussaddy A, Levy A, Strbian D, Sundararajan S, Berthelet F, Lanthier S. Inflammatory Cerebral Amyloid Angiopathy, Amyloid-beta-Related Angiitis, and Primary Angiitis of the Central Nervous System: Similarities and Differences. Stroke. 2015; 46:e210–213. [PubMed: 26185185]
39. Chung KK, Anderson NE, Hutchinson D, Synek B, Barber PA. Cerebral amyloid angiopathy related inflammation: three case reports and a review. J Neurol Neurosurg Psychiatry. 2011; 82:20–26. [PubMed: 20935328]
40. Auriel E, Charidimou A, Gurol ME, Ni J, Van Etten ES, Martinez-Ramirez S, Boulouis G, Piazza F, DiFrancesco JC, Frosch MP, Pontes-Neto OV, Shoamanesh A, Reijmer Y, Vashkevich A, Ayres AM, Schwab KM, Viswanathan A, Greenberg SM. Validation of Clinicoradiological Criteria for the Diagnosis of Cerebral Amyloid Angiopathy-Related Inflammation. JAMA Neurol. 2016; 73:197–202. [PubMed: 26720093]
41. Salvarani C, Hunder GG, Morris JM, Brown RD Jr, Christianson T, Giannini C. Abeta-related angiitis: comparison with CAA without inflammation and primary CNS vasculitis. Neurology. 2013; 81:1596–1603. [PubMed: 24078731]
42. Eng JA, Frosch MP, Choi K, Rebeck GW, Greenberg SM. Clinical manifestations of cerebral amyloid angiopathy-related inflammation. Ann Neurol. 2004; 55:250–256. [PubMed: 14755729]
43. Kinnecom C, Lev MH, Wendell L, Smith EE, Rosand J, Frosch MP, Greenberg SM. Course of cerebral amyloid angiopathy-related inflammation. Neurology. 2007; 68:1411–1416. [PubMed: 17452586]
44. Rigby H, Easton A, Bhan V. Amyloid beta-related angiitis of the central nervous system: report of 3 cases. Can J Neurol Sci. 2011; 38:626–630. [PubMed: 21672703]
45. Ryan NS, Lashley T, Revesz T, Dantu K, Fox NC, Morris HR. Spontaneous ARIA (amyloid-related imaging abnormalities) and cerebral amyloid angiopathy related inflammation in presenilin 1-associated familial Alzheimer's disease. J Alzheimers Dis. 2015; 44:1069–1074. [PubMed: 25408217]
46. Morelli L, Wei L, Amorim A, McDermid J, Abee CR, Frangione B, Walker LC, Levy E. Cerebrovascular amyloidosis in squirrel monkeys and rhesus monkeys: apolipoprotein E genotype. FEBS Lett. 1996; 379:132–134. [PubMed: 8635577]
47. Seripa D, D'Onofrio G, Panza F, Cascavilla L, Masullo C, Pilotto A. The genetics of the human APOE polymorphism. Rejuvenation Res. 2011; 14:491–500. [PubMed: 21958003]
48. Rannikmae K, Kalaria RN, Greenberg SM, Chui HC, Schmitt FA, Samarasekera N, Al-Shahi Salman R, Sudlow CL. APOE associations with severe CAA-associated vasculopathic changes: collaborative meta-analysis. J Neurol Neurosurg Psychiatry. 2014; 85:300–305. [PubMed: 24163429]
49. Geula C, Nagykery N, Wu CK. Amyloid-beta deposits in the cerebral cortex of the aged common marmoset (Callithrix jacchus): incidence and chemical composition. Acta Neuropathol. 2002; 103:48–58. [PubMed: 11837747]
50. D'Angelo OM, Dooyema J, Courtney C, Walker LC, Heuer E. Cerebral amyloid angiopathy in an aged sooty mangabey (Cercocebus atys). Comp Med. 2013; 63:515–520. [PubMed: 24326228]
51. Vite CH, Head E. Aging in the canine and feline brain. Vet Clin North Am Small Anim Pract. 2014; 44:1113–1129. [PubMed: 25441628]
52. Fast R, Rodell A, Gjedde A, Mouridsen K, Alstrup AK, Bjarkam CR, West MJ, Berendt M, Moller A. PiB Fails to Map Amyloid Deposits in Cerebral Cortex of Aged Dogs with Canine Cognitive Dysfunction. Front Aging Neurosci. 2013; 5:99. [PubMed: 24416017]

53. Colle MA, Hauw JJ, Crespeau F, Uchihara T, Akiyama H, Checler F, Pageat P, Duykaerts C. Vascular and parenchymal Abeta deposition in the aging dog: correlation with behavior. Neurobiol Aging. 2000; 21:695–704. [PubMed: 11016539]

54. Droby A, Lukas C, Schanzer A, Spiwoks-Becker I, Giorgio A, Gold R, De Stefano N, Kugel H, Deppe M, Wiendl H, Meuth SG, Acker T, Zipp F, Deichmann R. A human post-mortem brain model for the standardization of multi-centre MRI studies. Neuroimage. 2015; 110:11–21. [PubMed: 25595502]

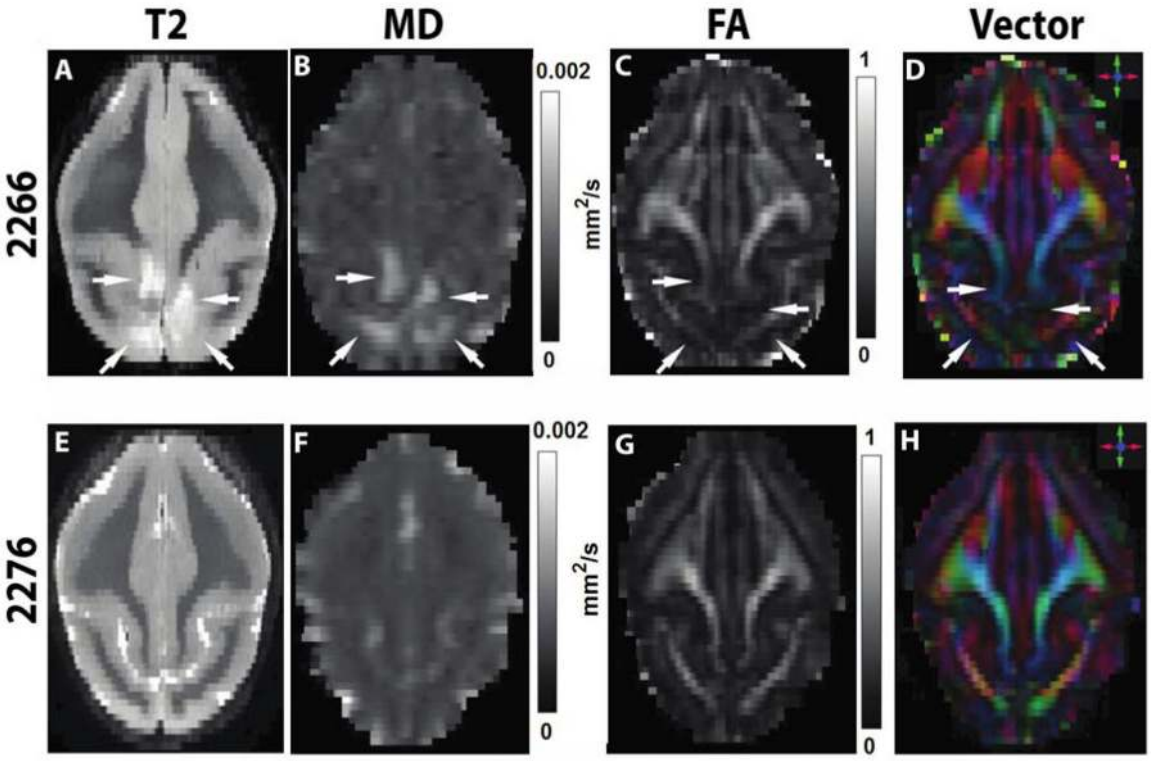

Figure 1. MRI of ARIA-E

Horizontal (axial) MR images (rostral is at the top) show bilateral hyperintense regions in the occipital lobes (arrows) in a T2-weighted scan of affected animal 2266 (**A**) compared to unaffected animal 2276 (**E**). Mean diffusivity (MD) is increased in the abnormal region of 2266 (**B** vs. **F**). Fractional anisotropy (FA; **C, G**) and the colorized vector maps (**D, H**) indicate a diminution of white matter integrity in the abnormal site. For clarity, all images in this report show the right hemisphere on the right.

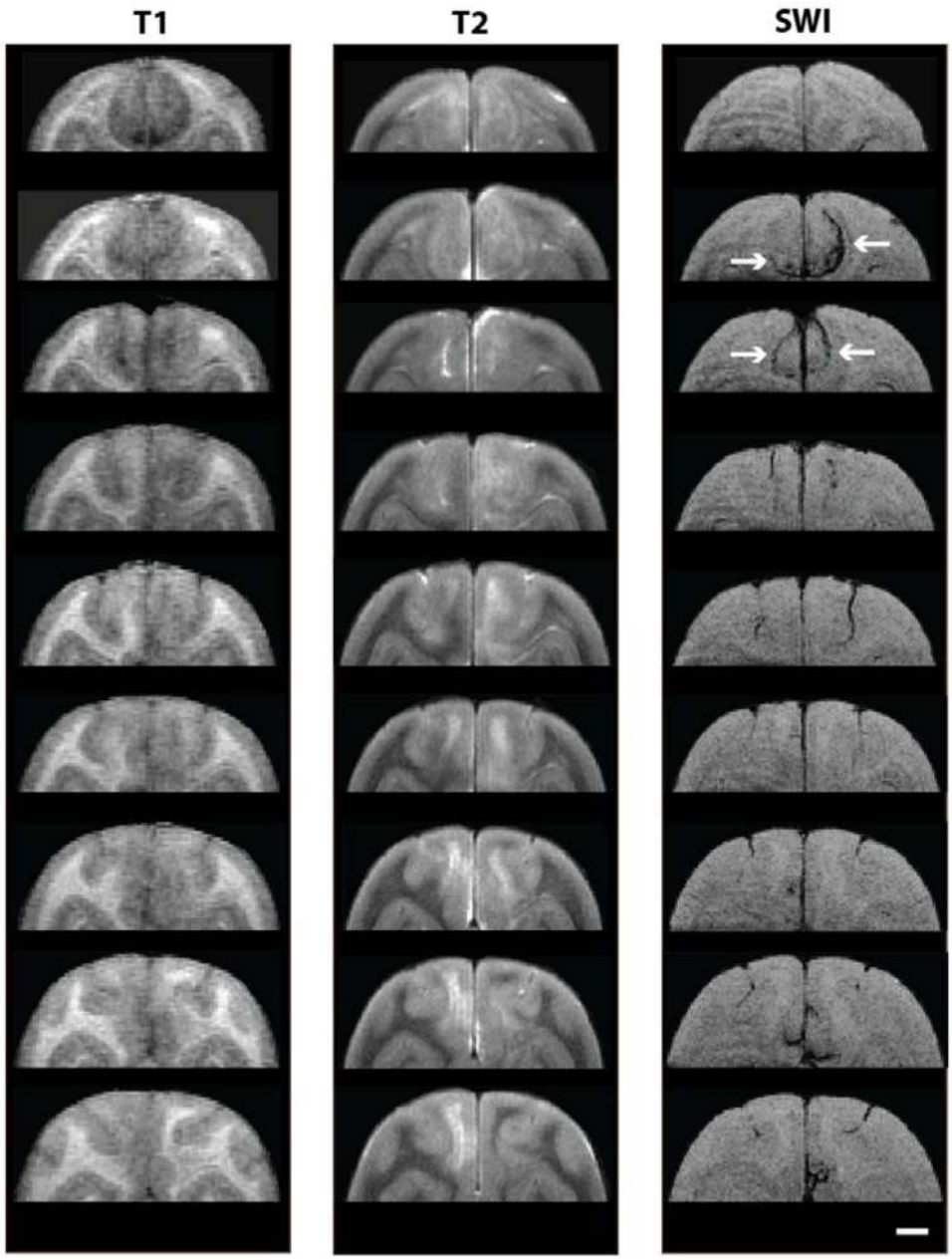

Figure 2. Coronal depiction of ARIA

T1-, T2-, and SWI-weighted MR images of ARIA-E and ARIA-H are shown at multiple coronal levels of the dorsal parieto-occipital cortex in squirrel monkey 2266 (1mm slice intervals). Both abnormalities extended for several millimeters along the rostro-caudal axis. Signal hypointensities corresponding to ARIA-H are marked by arrows at two coronal levels in the SWI column. Scale bar = 4mm.

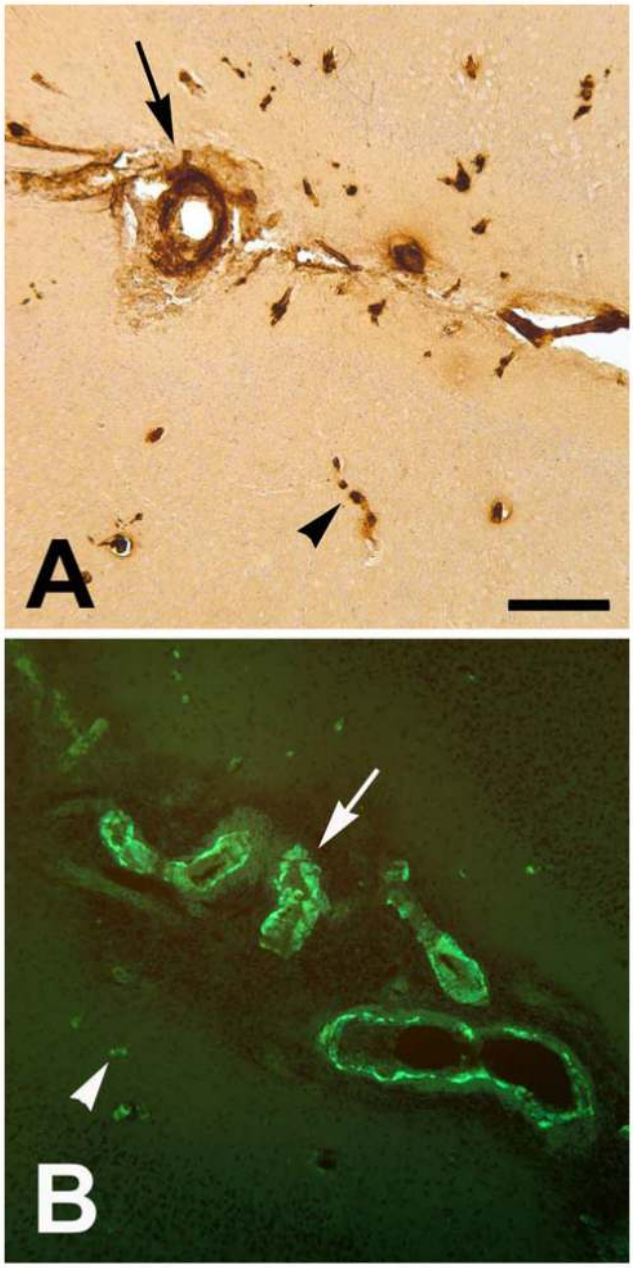

Figure 3. β-Amyloid in cerebral blood vessels

CAA in the parieto-occipital sulci and adjacent parenchyma of squirrel monkey 2266. Large vessels (arrows) and capillaries (arrowheads) were stained using antibody 6E10 (**A**; left hemisphere) and with Thioflavin-S (**B**; right hemisphere). CAA was present throughout the rostro-caudal extent of the forebrain, as is typical of aged squirrel monkeys. Scale bar = 200 μm for both panels.

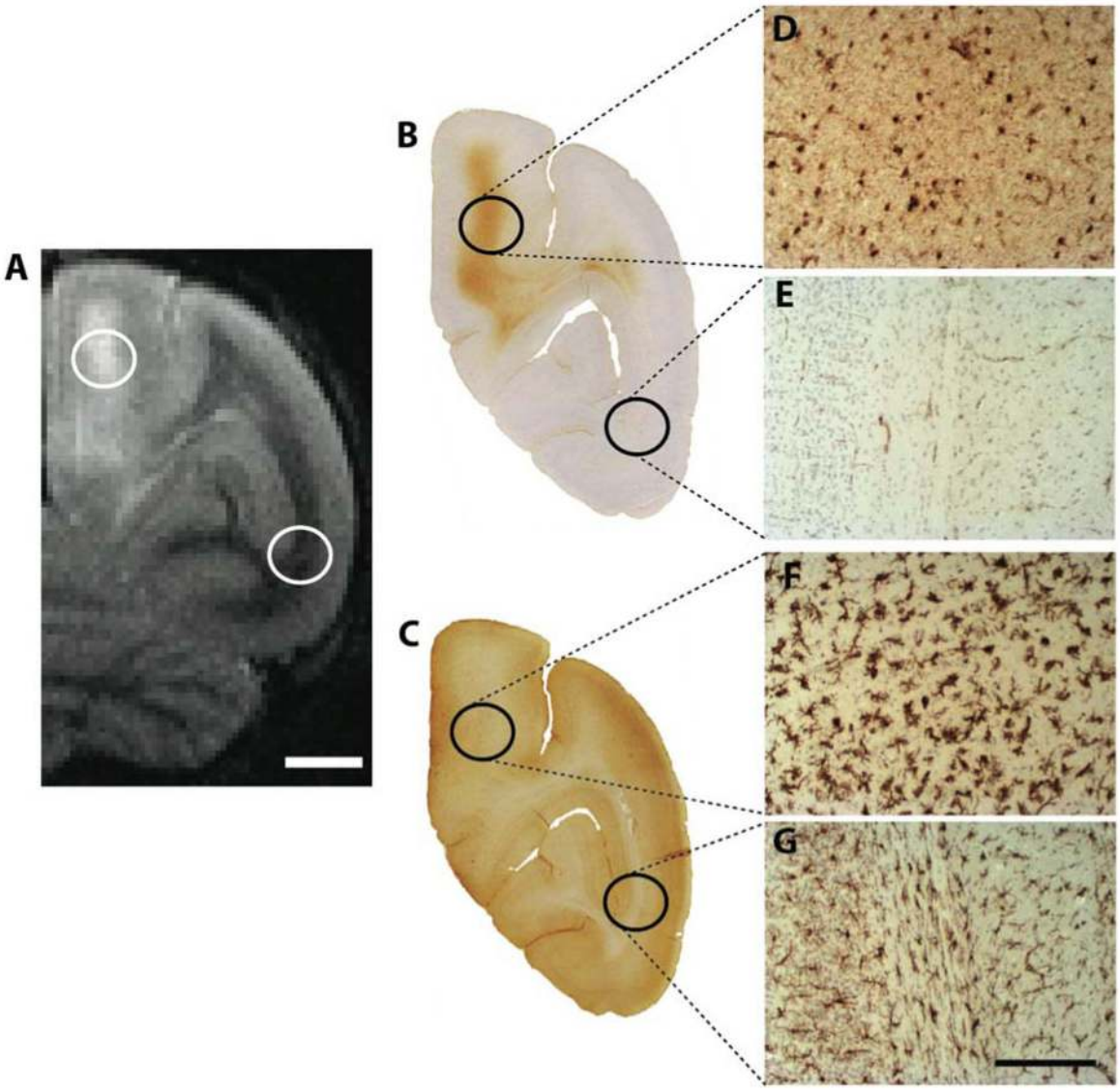

Figure 4. ARIA-associated gliosis

Reactive gliosis is shown in right hemispheric regions affected by ARIA-E in animal 2266. Brain sections at the coronal level corresponding to the T2-weighted MRI image in panel **A** were immunohistochemically stained for markers of astrocytes (**B**) and microglia (**C**). Higher magnification photomicrographs of reactive (hypertrophic) astrocytes (**D**) and microglia (**F**) in the ARIA-E-affected brain region compared to an unaffected region in the ventrolateral cortex as an internal control (**E** and **G**, respectively). Scale bar in A = 4 mm; Scale bar in G = 300 μm and applies to D-G.

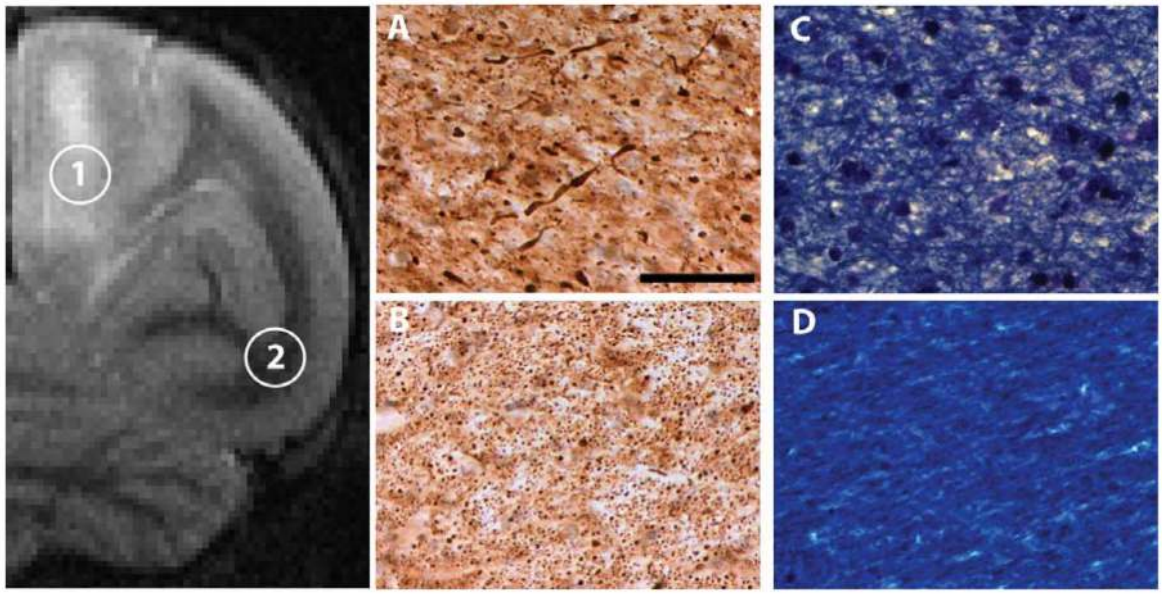

Figure 5. ARIA-associated white matter changes

Axonal phosphorylated neurofilaments (antibody SMI-31) were detected immunohistochemically in the right-hemispheric ARIA-E region (#1 in the T2-weighted image) of dorsomedial white matter (**A**) and in a normal-appearing ventrolateral region (#2 and panel **B**) of animal 2266. The damaged axons (as seen in panel A) were accompanied by a disruption of myelin integrity (Luxol Fast Blue) in the ARIA-E region (**C**) as compared to the control region (**D**). Scale bar in A = 200 μm and applies to A-D.

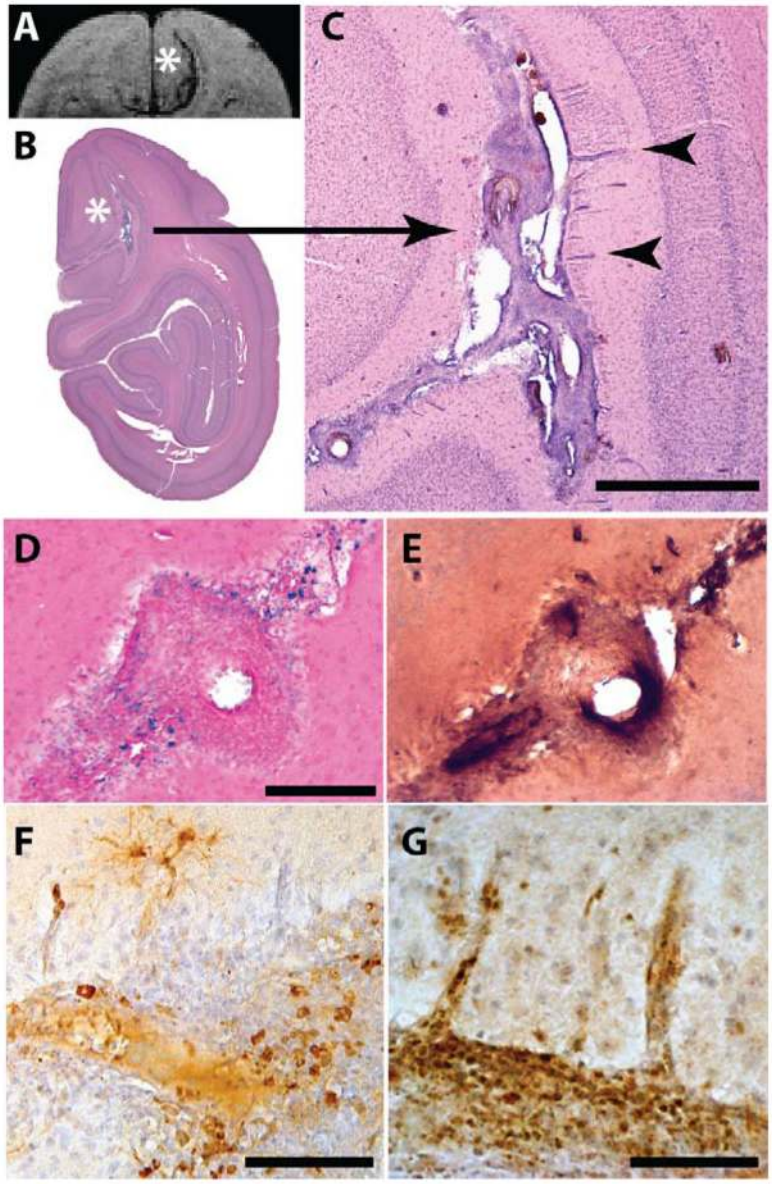

Figure 6. Hemosiderin deposition and inflammation

In the region of the right-hemispheric SWI hypointensity (to the right of the asterisk in panel **A**) in animal 2266, an abnormal cell-rich matrix is present in the parieto-occipital sulcus (shown at low magnification in **B** and higher magnification in **C**; hematoxylin and eosin stain). Note the perivascular accumulation of leukocytes (cuffing) around blood vessels penetrating the parenchyma of the brain (2 cuffed vessels are indicated by arrowheads in **C**; their intense bluish appearance denotes the presence of abundant, hematoxylin-stained inflammatory cells). Panel **D** shows hemosiderin deposition (blue) surrounding a sulcal blood vessel in the ARIA-H region (Perls' stain for ferric iron), and panel **E** shows the same vessel immunostained for Aβ (antibody 6E10). Panel **F** shows CD68-immunoreactive macrophages and panel **G** shows CD3-reactive T-lymphocytes in the sulcal matrix and

adjacent cortex (brown immunostain and hematoxylin counterstain in both). Bars = 1mm in C, 200 μm in D (which also applies to E), 200 μm in F, and 100 μm in G.

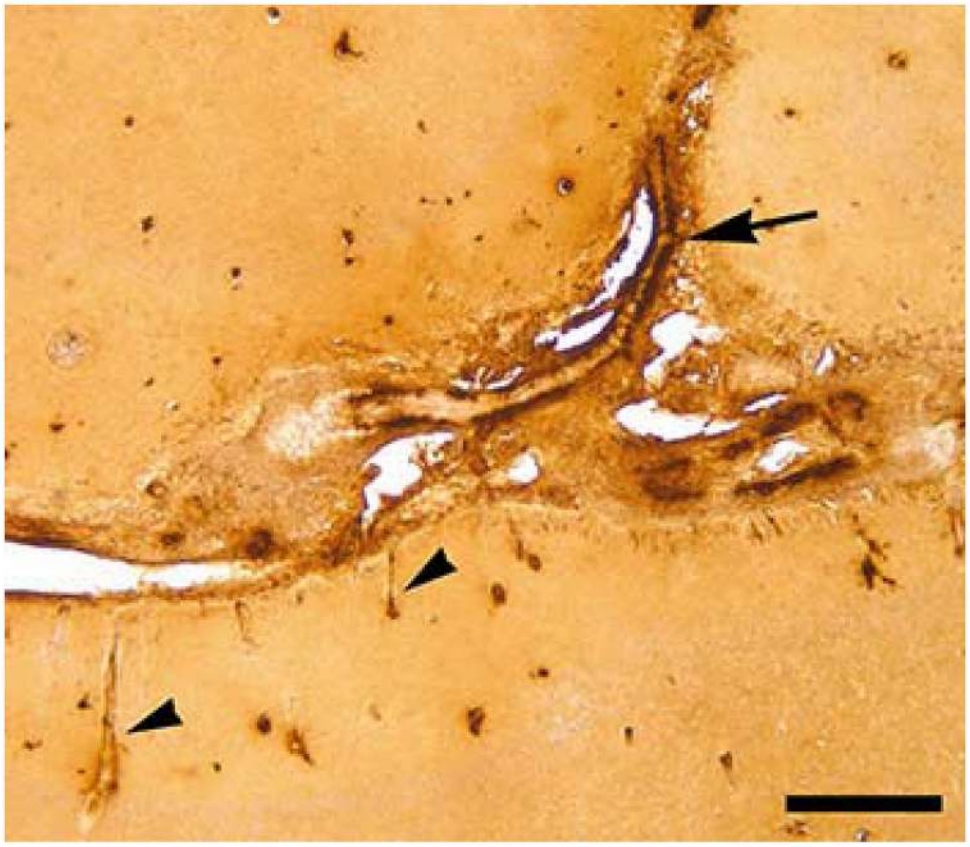

Figure 7.

An Aβ-immunoreactive sulcal blood vessel (arrow) is partially embedded in an abnormal matrix consisting largely of immune/inflammatory cells (material just below the vessel; see also Figure 6) in the ARIA-affected area of animal 2266; two immunoreactive penetrating vessels are denoted by arrowheads, and a number of Aβ-immunoreactive capillaries are present in the cortical parenchyma. Antibody 6E10; Bar = 400μm.

Table

The extent of Aβ-immunoreactive lesions in the cerebral vasculature (CAA) and parenchyma (Aβ plaques) in the analyzed cohort of squirrel monkeys. Lesion load was determined by consensus of three independent observers using photographs as standards for the stages of deposition.

Cerebral Aβ Load in Four Squirrel Monkeys

Subject	Sex	Age (years)	Aβ-Immunoreactive Lesions	
			CAA	Aβ plaques
2266	F	19	++++	++++
2276	F	19	++++	++
2504	F	16	++	+
3237	F	13	+	+

(+): minimal but detectable Aβ deposition; (++++): heavy Aβ deposition.